IVIM MRI of the Placenta

Paddy J. Slator [1], Jana Hutter [2,3], Eleftheria Panagiotaki [1], Mary A. Rutherford [2], Joseph V. Hajnal [2,3], Daniel C. Alexander [1,4]*
1. Centre for Medical Image Computing and Department of Computer Science, University College London, London, UK
2. Centre for the Developing Brain, King's College London, London, UK
3. Biomedical Engineering Department, King's College London, London, UK
4. Clinical Imaging Research Centre, National University of Singapore, Singapore
**p.slator@ucl.ac.uk*

1.1 INTRODUCTION

The placenta enables the transfer of oxygen and nutrients to the growing fetus, and is vital to the lifelong health of both mother and child [1,2]. It is highly vascular, contains large volumes of maternal and fetal blood, and undergoes major structural and functional changes across the 40 weeks of gestation. It therefore presents unique challenges, and opportunities for IVIM MRI.

1.1.1 *Placental markers of pregnancy complications*

Many major pregnancy complications are associated with placental malfunction [3]. Deviations in blood flow can disrupt the transfer of oxygen and nutrients to the developing fetus, eventually leading to complications such as fetal growth restriction [4–6] (FGR, defined as growth below the genetic potential of the fetus) and pre-eclampsia [7,8] (PE, a disease characterized by elevated maternal blood pressure and proteinuria). Despite these underlying placental aetiologies, both FGR and PE are difficult to detect before the onset of symptoms. In other words, at the point of FGR or PE diagnosis there has already been substantial inhibition of placental function. Biomarkers which quantify placental

development - with their potential for prediction, earlier diagnosis, and better management of high-risk pregnancies - are therefore of great importance.

1.1.2 *Imaging markers of pregnancy complications*

Ultrasound is currently the main modality for pregnancy monitoring. A wide range of ultrasound-derived biomarkers are currently used in the clinic, such as fetal biometry, heart rate, amniotic fluid volume, and Doppler ultrasound of the umbilical cord and uterine arteries. FGR is generally diagnosed by a combination of Doppler ultrasound of the umbilical cord and uterine arteries, and fetal biometry abnormalities [9–11]. However, there are many limitations to placental ultrasound: it has a small field of view, limiting whole organ assessment especially later in gestation, low contrast, and provides limited functional information [12].

1.1.3 *Challenges and unique potential of placental MRI*

MRI can probe both structure (what tissue is present and its configuration) and function (e.g. blood flow, oxygenation, and nutrient exchange). It therefore offers a unique perspective on the placenta, and has the potential to address the limitations of ultrasound. MRI has been recently shown to offer improvements in sensitivity and specificity, for example mean placental T2* is a stronger predictor of low birth weight than Doppler ultrasound [13]. However, there are a number of factors that limit the utility of placental MRI. These include maternal and fetal motion, uterine contractions, and magnetic field inhomogeneity. It is likely that the uniqueness of the placenta means that bespoke solutions to these problems are required. Recent work has made significant progress towards these goals [14–17], hence increasing the clinical viability of placenta MRI.

1.1.4 *Diffusion MRI of the placenta*

In particular, diffusion MRI (dMRI) - with its potential for non-invasive assessment of tissue microstructure and microcirculation - is emerging as a promising tool for placental assessment. There are a small, but growing, number of in-vivo human placenta dMRI studies in the literature. A majority of these studies have utilized IVIM MRI (we review these later in the chapter). In addition, placenta dMRI studies have been performed using apparent diffusion coefficient (ADC) [18–21] and diffusion tensor imaging (DTI) [22] models.

1.1.5 *Placenta structure*

The placenta attaches to the maternal uterine wall, and connects to the fetus via the umbilical cord. It is typically around 20cm across and 2cm thick, and consists of 30-40 lobules (also known as cotyledons). Each lobule contains of 1-2 functional units containing a paired maternal spiral artery and fetal villous tree. Figure 1 is a schematic of the placenta structure and outlines the principle blood flow routes. Fetal villous trees consist of a large stem villous attached to the chorionic plate; this stem subsequently branches into a network of smaller intermediate villi, which further divide into a network of capillarized terminal villi. Maternal spiral arteries and decidual veins are located immediately adjacent to the placenta in the uterine wall, which consists of various fibrous cell types, and trophoblastic cells.
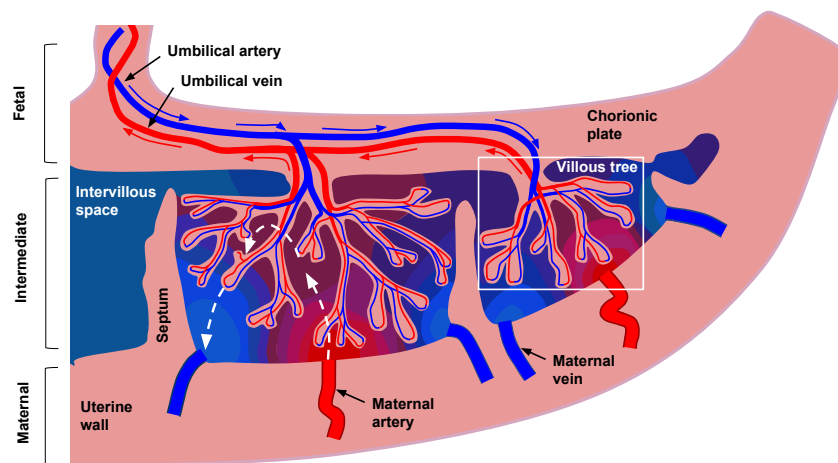
Figure 1. Schematic representation of blood flow through the placenta and surrounding tissue. Blue and red arrows show the flow directions of oxygenated (red) and deoxygenated (blue) fetal blood through the placental vasculature. For clarity, only the largest villi are included. Dashed white arrows show idealized flow lines through intervillous space for maternal blood. Idealized oxygenation states are represented by the red to blue color gradient. Figure and caption from [23], used under the CC BY license.

1.1.5.1 *Movement of blood*

There are two non-mixing blood types in the placenta - fetal and maternal - both of which have very different flow characteristics. Fetal blood resides in the fetal vasculature, and perfuses at high pressure through the convoluted villous network. On the other hand, and quite uniquely, maternal blood doesn't flow within vasculature. Instead, it flows at low pressure through spiral arteries into the intervillous space, submerging the fetal villous trees and therefore facilitating oxygen exchange with fetal blood across the villous tree surface.

1.1.5.2 *How the placenta structure affects the dMRI signal*

Due to the unique circulatory structures, it is not immediately clear how the placental dMRI signal will be attenuated at different b-values. Our thoughts on how placental structure, microstructure, and microcirculation may affect the dMRI signal are as follows. We expect that blood flowing incoherently within fetal vasculature exhibits a pseudo-diffusive effect at the voxel scale, and hence contributes a fast-attenuating dMRI signal component. We also expect a slow-attenuating dMRI signal component due to water in tissue, such as fetal villous tree walls. It is far from clear how maternal blood flow will impact the dMRI signal. It may exhibit fast incoherent flow on the voxel scale when within vasculature, e.g. spiral arteries and decidual veins. Therefore a fast-attenuating component to the dMRI signal is likely within the uterine wall. However, once it has entered intervillous space, its behaviour is very different. Any coherent flow of maternal blood should cause little signal attenuation, however diffusion within this flow should cause some signal attenuation - with a diffusivity comparable to water at body temperature $(3 \times 10^{-3} \text{ mm}^2 \text{ s}^{-1})$. Additionally, percolation of maternal blood through highly convoluted spaces proximal to fetal villi (in order to facilitate oxygen exchange) may appear incoherent at the voxel scale. If this is the case, it is very difficult to know the speed at which this blood would be percolating, and hence what dMRI signal component (fast-attenuating, slow-attenuating or otherwise) this would affect. Previous work in mouse placentas by Solomon et al. sheds some light on the problem [24]. They found that maternal blood had near free diffusion behaviour, whereas fetal blood flows two orders of magnitude quicker. However, whether this observation translates to human placentas remains unclear.

1.1.5.3 *Development across gestational age*

The placenta undergoes major functional and structural changes across the 40 weeks of gestation in order to support the developing fetus. For example terminal villi - the principal location of oxygen exchange - develop mainly after 20 weeks [25]. Additionally, calcification generally begins from week 37 onwards, and premature onset has been linked to

adverse maternal and fetal outcomes [26–28]. These changes offer both challenges and unique opportunities. Quantitative methods need to be sensitive to the full range that parameters can take over gestation. If such methods could accurately characterize these physiological and pathological developments this would be of great interest clinically. IVIM MRI provides a unique tool for working towards this goal.

1.2 IVIM IN THE PLACENTA

The first in-vivo measurements of IVIM MRI parameter values (in fact, the first applications of dMRI) in the human placenta were presented in two publications in 2000 [29,30]. The first [29], presents IVIM results from eleven healthy subjects to give an idea of the ranges and trends over gestation of all three IVIM parameters - the perfusion fraction, pseudo-diffusivity and diffusivity. FGR cases were scanned in the second article, and an IVIM-derived parameter was identified - the difference in perfusion fraction between outer and inner placental ROIs - that was lower in FGR pregnancies [30].

   In subsequent placental studies, IVIM has remained the most common model for interpreting dMRI data. These papers have generally followed one of the approaches in these first two papers: try to characterize the trajectory of IVIM parameters across gestational age, or identify an IVIM parameter which is significantly altered due to pathology. Table 1 gives a summary of the published studies of IVIM MRI applied to the in-vivo human placenta.

   Table 1. Reported diffusion MRI parameters in the placenta for in-vivo human pregnancies. Values are reported as either mean $\pm$ SD, or median (IQR). All studies were performed at 1.5 T, excluding both studies by Moore *et al.* (0.5 T), and some of the subjects in Jakab et al. (3 T). Each study includes a variety of subjects, either with or without disease, we refer the reader to the original studies for full details. Capuani *et al.* [31] did not report parameter values in the text; the values we present were read from the figures. We have not included a second paper by Sohlberg *et al.* [32], as it

contains the same subjects as [33].

Reference	b-values (s mm^{-2})	No. of subjects	Pseudo-diffusivity (10^{-3} mm^2 s^{-1})	Diffusivity (10^{-3} mm^2 s^{-1})	Perfusion fraction (%)
Moore *et al.* [29]	0, 0.2, 3, 15, 47, 80, 115, 206, 246, 346, 468	11	57 ± 41	1.7 ± 0.5	26 ± 6
Moore *et al.* [30]	0, 0.2, 3, 15, 47, 80, 115, 206, 246, 346, 468	20		1.7 ± 0.9 (inner ROI) 1.4 ± 0.8 (outer ROI)	25 ± 8 (inner ROI) 35 ± 11 (outer ROI)
Derwig *et al.* [34]	0, 0.7, 3, 9, 18, 32, 54, 88, 147, 252, 500	37			36.2 (9.6)
Sohlberg *et al.* [33]	0, 200, 400, 600, 800	32			29 (8)
You *et al.* [35]	0, 25, 50, 114, 243, 500, 543, 800, 900	16			58 ± 11 (fetal ROI) 56 ± 13 (maternal ROI)
Capuani *et al.* [31]	0, 50, 100, 150, 400, 700, 1000	30	13 ± 1	1.5 ± 0.15	34 ± 3
Siauve *et al.* [36]	0, 15, 47, 80, 115, 206, 246, 346, 468, 700, 1000	23	21.22 ± 11.18	1.74 ± 0.30	39.37 ± 10.90
Jakab et al. [37]	0, 10, 20, 30, 40, 60, 80, 100, 150, 200, 300, 400, 500, 600, 700, 800, 900	33	4.77 ± 3.33		29 ± 8

1.2.1 *Trends across gestational age*

There are two main reasons for characterizing biomarker trends across gestation. Since many change significantly throughout normal gestational aging, knowledge on typical biomarker trends is a necessary requirement

to identify deviation. Additionally, we know that the placenta undergoes dramatic microstructural changes across gestation. If we can identify the dMRI-derived parameters which best capture these changes, it follows that these will be good candidates for detecting pathological microstructural changes.

There is variability in the reported trends for IVIM MRI parameters across gestational age. Three studies - all of which began scanning at 22 weeks - have shown a clear decrease in perfusion fraction across gestation [29,33,35]. Siauve et al. scanned at earlier gestations (starting at 16 weeks) and found an increase in perfusion fraction between 16 and 22 weeks of GA, stability between 22 and 28 weeks, then a decrease [36]. On the other hand, two recent papers have shown an apparent increase in perfusion fraction across gestation [31,37].

There are a number of factors which could cause this inter-study variability. These include the lack of a common protocol, variability in ROI selection, different GA ranges, and variation in the types of pregnancy included. For example, Capuani et al. used small ROIs within the placenta - rather than a whole organ average - to calculate perfusion fraction values. Compared to other studies, Jakab et al. have a much larger range in perfusion fraction values, which may reflect differences in the dMRI protocol or model fitting procedure. Clearly further studies are necessary in order to account for these discrepancies. How these factors specifically affect the observed trend in IVIM perfusion fraction across gestation is an important area for future work, and of crucial importance for any future use as biomarkers.

1.2.2 *Parameter variation with pathology*

The ultimate aim of IVIM MRI in the placenta is to identify parameters - or combinations thereof - which are sensitive to the presence or severity of pathology. Thus far, although we should emphasize the small number of studies, IVIM-derived parameters have shown reasonable discrimination between normal and pathological placentas. For example, the perfusion fraction appears significantly lower in placentas associated with FGR [30,32,34], and early onset PE [33]. Additionally two studies

show that ADC - which averages over IVIM effects - was decreased in FGR [19,21]. However, it should be noted that the choice of b-values heavily affects the inferred ADC values [18].

1.3 ANISOTROPIC IVIM IN THE PLACENTA

Whilst standard models for analyzing dMRI data, such as IVIM, ADC, and DTI, have shown promise in the placenta, it has been shown in other tissues that advanced microstructural models can extract more specific biophysically-linked parameters from the signal. We recently undertook a study to assess which microstructural models best explain dMRI data in the placenta [23].

1.3.1 *dMRI scans*

We scanned 9 healthy pregnant subjects with a rich, multi-shell, multi-directional dMRI protocol. The three principal gradient directions were scanned at b=15, 25, 80, 115, 206, 246, 346 s mm^{-2}, eight directions were obtained at b=40, 400, 1000, 2000 s mm^{-2}, and there were six b=0 images. We used this acquisition - which is much richer than would typically be available - in order to assess the most expressive models which the placental dMRI signal potentially supports.

1.3.2 *Modelling*

The models we fit to the data were motivated by our predictions of how placental structure and microstructure will attenuate the dMRI signal (i.e. Section 1.1.5.2 . We chose a set of 14 microstructural models, the majority of which consist of two compartments separately modelling the fast-attenuating (primarily associated with perfusion) and slow-attenuating (primarily associated with diffusion) signal components.

In "standard" IVIM MRI, perfusion and diffusion compartments are both considered to be isotropic. This may not hold in the placenta, for example in areas with fibrous cells or where vasculature has a coherent orientation. We therefore include models which allow anisotropy in

perfusion and diffusion compartments, and can therefore be considered anisotropic extensions to IVIM. We found it informative to categorize our models depending on the anisotropy of these two compartments. For example, we use "anisotropic-isotropic" to refer to models with anisotropic perfusion compartment and isotropic diffusion compartment.

All models are combinations of compartments as described in [38], such as ball, stick, zeppelin, and tensor. "Ball" represents an isotropic diffusion compartment (i.e. an ADC model). A "tensor" compartment models the signal using a full diffusion tensor, and "zeppelin" is a cylindrically symmetric tensor. A "stick" is maximally anisotropic, assuming that water only diffuses in a single direction. Models are built up using combinations of these compartments, again following the terminology in [38], for example the standard IVIM model is "ball-ball".

An example anisotropic IVIM model is stick-zeppelin, a two-compartment model which contains anisotropic perfusion and diffusion compartments. The signal is given by

$$S(b) = f \exp\left(-b d_p \left(\boldsymbol{n_p} \cdot \boldsymbol{G}\right)^2\right) + (1 - f) \exp(-b \boldsymbol{G^T D G})$$

where f is the perfusion fraction, b is the b-value, d_p is the diffusivity in the stick principle direction, $\boldsymbol{n_p}$ is the stick principle direction, $\boldsymbol{G}$ is the gradient direction, and $\boldsymbol{D}$ is a cylindrically symmetric tensor (i.e. "zeppelin"). The first term in the signal equation therefore models perfusion effects using a stick compartment, and the second term models diffusion effects using a zeppelin compartment.

To see which model best explained the placenta dMRI signal, we calculated a model selection statistic (the Bayesian information criterion) for all 14 models voxel-by-voxel across all 9 subjects.

1.3.3 *Results*

Figure 2 shows voxelwise model selection results. Clearly, anisotropic IVIM models best explain the dMRI signal in a majority of voxels across all subjects, with the best model categories being anisotropic-anisotropic and anisotropic-isotropic. In other words, the best models have anisotropic perfusion compartment, and either isotropic or anisotropic

diffusion compartment. **Error! Reference source not found.** reveals the spatial pattern of the anisotropy of the diffusion compartment. This pattern is consistent with the underlying physiology: there is generally isotropy within the placenta - which may be due to large maternal blood pools, and anisotropy within the uterine wall and chorionic plate - potentially reflecting fibrous cell structures.
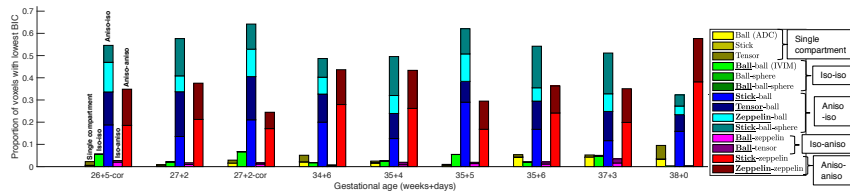

Figure 2. Model selection results over 9 placenta dMRI scans. Bar plots show the proportion of voxels within a placental ROI where each model had the lowest Bayesian information criterion. Subjects are labelled by gestational age, with "-cor" indicating that the placenta was scanned coronally. The perfusion model compartment is emphasized in the legend text. Image adapted from [23], used under the CC BY license.
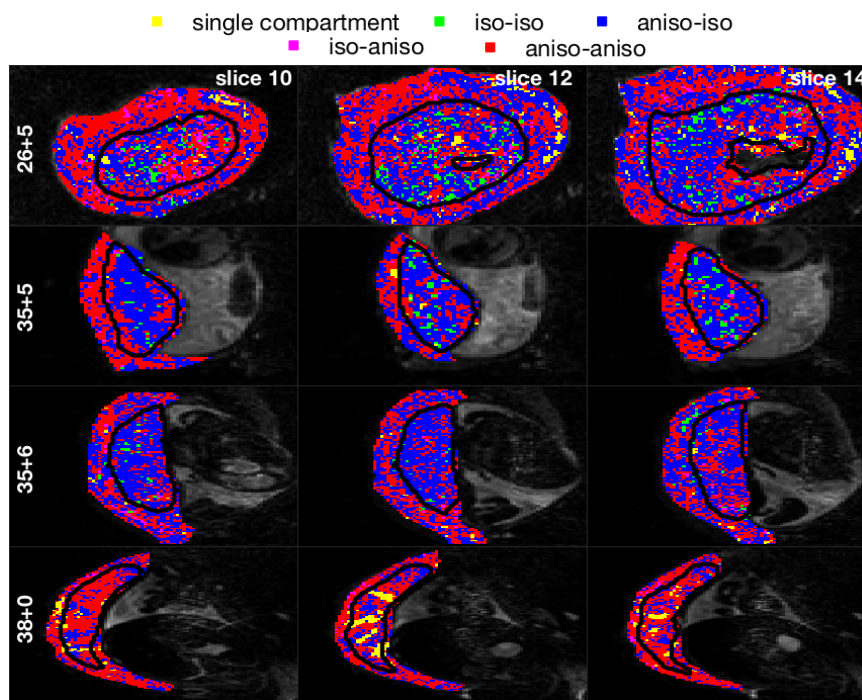
Figure 3. Mapping the spatial pattern of model selection results. Each row displays three slices for a single subject, labelled by gestational age (weeks+days). Voxels are colored according to the category of model with the lowest BIC in that voxel. Models are grouped according to the isotropy of the perfusion and diffusion compartments respectively, for example "aniso-iso" refers to models with anisotropic perfusion compartment and isotropic diffusion compartment. From [23], used under the CC BY license.

Figure 4 displays DTI and IVIM parameter maps for 4 subjects. We see similar patterns in maps across all subjects, and these are consistent with the physiology of the placenta and surrounding tissue. For example, we saw consistently high diffusivity in the uterine wall (e.g. Figure 4, first column). These areas also had high IVIM perfusion fraction (Figure 4, fourth column) suggesting they reflect areas with high volumes of

perfusing blood. Fractional anisotropy (FA) and direction encoded colour (DEC) maps show high anisotropy in the areas around the placenta (Figure 4, columns 2 and 3) - likely due to the prevalence of fibrous cells in the uterine wall and chorionic plate.
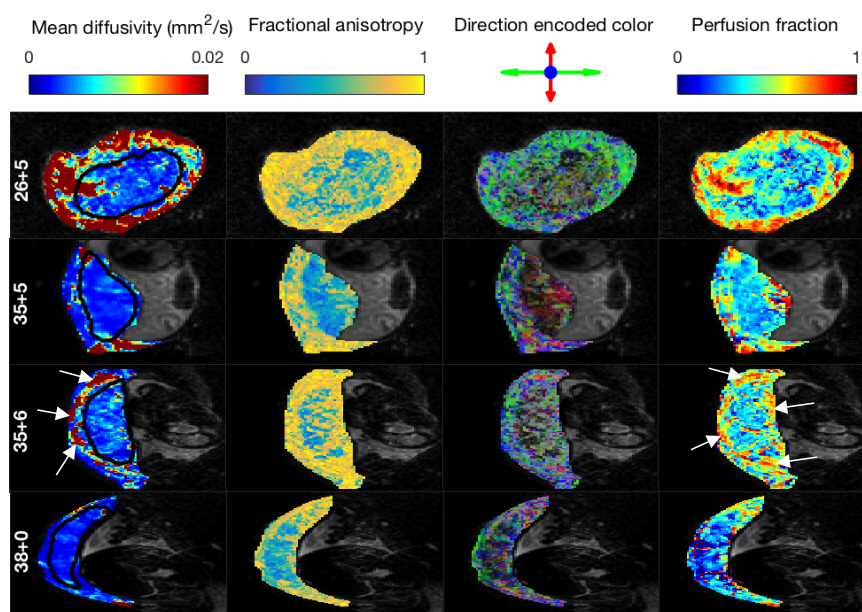

Figure 4. Parameter maps derived from DTI and isotropic IVIM model fits. Each row displays maps for a single slice from one subject, labelled by gestational age (weeks+days). Arrows in row 3 highlight areas of high diffusivity and high perfusion at the boundary of the placenta. From [23], used under the CC BY license.

We display stick-zeppelin - which performed consistently well in model selection - parameter maps in Figure 5. These maps reveal more information than can be accessed with the standard IVIM model (i.e ball-ball in our terminology). In particular, column 4 maps show the anisotropy of the slow-attenuating dMRI signal component - revealing high anisotropy in the uterine wall and chorionic plate. These models also provide zeppelin diffusivity, stick diffusivity and stick volume fraction

maps (columns 1-3) - analogous to diffusivity, pseudo-diffusivity and perfusion fraction respectively in the isotropic IVIM model.

Figure 5. Parameter maps derived from stick-zeppelin model fit. Each row displays maps for a single axial slice from one subject, labeled by gestational age (weeks+days). From [23], used under the CC BY license.

Finally, although we emphasize the small number of samples and the lack of longitudinal measurements from individual subjects, our study shows a decrease in the perfusion fraction across gestational age (Supporting Information in [23]). This is in agreement with [29,33,35], but disagrees with [31,37].

1.3.4 *Discussion*

Our analysis shows that, when using a rich dMRI protocol, anisotropic IVIM models explain the in-vivo human placenta dMRI signal better than

ADC, IVIM and DTI models. We found that the fast-attenuating signal component was anisotropic in nearly all voxels, which matches the interpretation that vasculature has a coherent structure. This orientation may be necessary to facilitate the transport of large volumes of blood - both maternal and fetal - into and out of the placenta. We also observed that the slow-attenuating signal component tended to be isotropic within the placenta - consistent with the lack of coherent tissue structure, and anisotropic in the areas surrounding the placenta - potentially reflecting the prevalence of fibrous tissue in the uterine wall and chorionic plate.

In future work, we will concentrate on the anisotropic IVIM models which best quantify placental microstructure and microcirculation. Stick-zeppelin and zeppelin-zeppelin had consistently high model selection ranking across the placenta and uterine wall, and hence show high promise. Zeppelin-zeppelin is the more general model as, unlike a stick compartment, a zeppelin can model isotropic diffusion (when axial and radial tensor diffusivities are equal). However, stick-zeppelin has three fewer parameters and is hence easier to fit to the data. Both models therefore have advantages in certain situations, our view is that zeppelin-zeppelin is preferable for very rich dMRI acquisition protocols, whereas stick-zeppelin is best for sparser acquisitions.

These observations naturally lead to another area for future development: designing dMRI protocols specifically to support these anisotropic IVIM models. The rich dMRI acquisition protocol utilized in this study is for discovery of the models that best explain the placental dMRI signal. Once these models have been identified, we can construct much more economical protocols suitable for clinical application.

1.4 DISCUSSION AND FUTURE DIRECTIONS

IVIM MRI - and anisotropic extensions - show promise as quantitative imaging methods in the placenta. However, there is much further work required to achieve the ultimate goal of translation into biomedical applications.

The IVIM perfusion fraction shows promise as a biomarker for FGR [30,32,34] and PE [33], and the ADC is decreased in FGR [19,21]. A

limitation of these studies is that they use parameter values averaged over the whole organ. Future development should harness the increased statistical power available by considering the distribution of quantitative measures across the whole organ, rather than averaging to a single descriptive statistic. Future work should also focus not only on whether dMRI-derived biomarkers are significantly different between control and disease groups, but also whether biomarkers can be used for diagnosis and prediction.

Another important topic is the effect of gestational age on dMRI-derived parameters. Previous work has shown that these parameters are highly sensitive to microstructural changes during normal placental development, but there is fundamental disagreement in the literature over the trends. If we do not have a good idea of the normal trajectories of these parameters, then we cannot accurately detect pathological changes. Future work should therefore aim to disentangle how pathology and gestational age affect biomarker values. This is likely to require development of analytical approaches which jointly consider these effects.

1.4.1 *Protocol optimization*

The utility of dMRI data depends on the choice of b-values and gradient directions. Given the observations from an initial cohort of 9 placental dMRI scans ([23], as outlined earlier in the chapter) we optimized the choice of gradient table [39]. Our approach was to separately optimize b-values and gradient directions in order to best assess the anisotropy in both perfusion and diffusion regimes. The optimization pipeline can be adjusted to comply with clinically limited scanning times.

Improvements in image post-processing are also important for IVIM MRI in the placenta. The majority of existing studies perform no motion correction, assuming alignment across dMRI volumes. This affects the visual quality of IVIM MRI parameter maps [40], and is presumably a major reason why most studies have focused on whole-organ averages of parameter values. Placental MRI motion correction is a difficult problem and requires correction of non-rigid motion [15]. Continued improvement

of motion correction algorithms should increase the utility of placental dMRI data.

1.4.2 *It's not just about the placenta!*

The placenta is a unique organ which contains both maternal and fetal tissue, and the exact nature of the maternal-placental boundary is debated [41]. Thus far dMRI and IVIM studies have tended to focus exclusively on the placenta, usually ignoring tissue immediately surrounding the organ. It seems likely that useful information can be extracted from measurements in these surrounding areas. In particular, maternal tissue in the uterine wall provides a rich source of information that should not be ignored, since the transport of maternal blood into the placenta through spiral arteries is critical to the health of the fetus. This view is supported a previous IVIM study, which showed reduced perfusion fraction in spiral arteries in pregnancies complicated by PE [42]. Fortunately, these surrounding areas are usually within the field of view of a placental scan, so the additional information comes for free.

1.4.3 *Joint diffusion-relaxometry*

The T2* signal strength in MRI depends (to some extent, [43]) on the concentration of oxygen in blood. This has been exploited in a number of placental studies [13,14,44,45]. There are also studies which have quantified T1 and T2 values in the placenta [46–49]. These studies demonstrated that T1, T2 and T2* values decreased across gestational age. An exciting avenue for future development is to combine diffusivity and relaxometry information to improve placental microstructure and microcirculation characterisation, as previously demonstrated with T2 and diffusivity [50].

1.4.4 *Histological validation*

The placenta is delivered at birth; there are hence unique opportunities to compare in-vivo dMRI measurements to histological observations.

However, there are a number of practical issues which first need to be addressed. The placenta is highly deformable, so matching the orientation and positioning of the placenta between MRI and histology would be challenging. Another issue relating to IVIM MRI is that there is no perfusion in the delivered placenta, so validation would have to focus on structural, rather than functional, properties. Despite these difficulties, there is clear scope for making initial progress in this area. A first goal might be to match dMRI measurements in cases with gross pathology - such as large infarctions or haemorrhage - with histological observations.

1.5 CONCLUSION

IVIM MRI shows much promise for studying microstructure and microcirculation in the human placenta and surrounding tissue structures. IVIM parameters are sensitive to both normal placental development, and pathological changes. Future work combining dMRI-derived parameters with data from other MRI modalities has the potential to increase overall sensitivity to placental viability. The ultimate aim is to develop quantitative imaging methods that can improve prediction, diagnosis, and monitoring of pregnancy complications.

ACKNOWLEDGEMENTS

BIBLIOGRAPHY

1.   Nelson DM. How the placenta affects your life, from womb to tomb. Am J Obstet Gynecol. Elsevier Inc.; 2015;213: S12–S13. doi:10.1016/j.ajog.2015.08.015
2.   Thornburg KL, Marshall N. The placenta is the center of the chronic disease

universe. Am J Obstet Gynecol. Elsevier Inc.; 2015;213: S14–S20. doi:10.1016/j.ajog.2015.08.030

3.   Latendresse G, Founds S. The Fascinating and Complex Role of the Placenta in Pregnancy and Fetal Well-being. J Midwifery Women's Heal. 2015;60: 360–370. doi:10.1111/jmwh.12344

4.   Vedmedovska N, Rezeberga D, Teibe U, Melderis I, Donders GGG. Placental pathology in fetal growth restriction. Eur J Obstet Gynecol Reprod Biol. 2011;155: 36–40. doi:10.1016/j.ejogrb.2010.11.017

5.   Mifsud W, Sebire NJ. Placental pathology in early-onset and late-onset fetal growth restriction. Fetal Diagn Ther. 2014;36: 117–128. doi:10.1159/000359969

6.   Veerbeek JHW, Nikkels PGJ, Torrance HL, Gravesteijn J, Post Uiterweer ED, Derks JB, et al. Placental pathology in early intrauterine growth restriction associated with maternal hypertension. Placenta. Elsevier Ltd; 2014;35: 696–701. doi:10.1016/j.placenta.2014.06.375

7.   Myatt L. Role of placenta in preeclampsia. Endocrine. 2002;19: 103–11. doi:10.1385/ENDO:19:1:103

8.   Roberts JM, Escudero C. The placenta in preeclampsia. Pregnancy Hypertens. 2012;2: 72–83. doi:10.1016/j.preghy.2012.01.001

9.   Kaponis A, Harada T, Makrydimas G, Kiyama T, Arata K, Adonakis G, et al. The importance of venous Doppler velocimetry for evaluation of intrauterine growth restriction. J Ultrasound Med. 2011;30: 529–545.

10.   Figueras F, Gratacós E. Update on the diagnosis and classification of fetal growth restriction and proposal of a stage-based management protocol [Internet]. Fetal Diagnosis and Therapy. Karger Publishers; 2014. pp. 86–98. doi:10.1159/000357592

11.   Alfirevic Z, Stampalija T, Dowswell T. Fetal and umbilical Doppler ultrasound in high-risk pregnancies [Internet]. Cochrane Database of Systematic Reviews. John Wiley & Sons, Ltd; 2017. doi:10.1002/14651858.CD007529.pub4

12.   Andescavage NN, du Plessis A, Limperopoulos C. Advanced MR imaging of the placenta: Exploring the in utero placenta–brain connection. Semin Perinatol. 2015;39: 113–123. Available: http://linkinghub.elsevier.com/retrieve/pii/S0146000515000051

13.   Sinding M, Peters DA, Frøkjær JB, Christiansen OB, Petersen A, Uldbjerg N, et al. Prediction of low birth weight: Comparison of placental T2* estimated by MRI and uterine artery pulsatility index. Placenta. Elsevier; 2017;49: 48–54. doi:10.1016/j.placenta.2016.11.009

14.   Schabel MC, Roberts VHJ, Lo JO, Platt S, Grant KA, Frias AE, et al. Functional imaging of the nonhuman primate Placenta with endogenous blood oxygen level-dependent contrast. Magn Reson Med. 2016;76: 1551–1562. doi:10.1002/mrm.26052

15.   Turk EA, Luo J, Gagoski B, Pascau J, Bibbo C, Robinson JN, et al. Spatiotemporal alignment of in utero BOLD-MRI series. J Magn Reson Imaging. 2017; doi:10.1002/jmri.25585

16.   Hutter J, Christiaens D, Deprez M, Cordero-Grande L, Slator PJ, Price AN, et al. Dynamic Field Mapping and Motion Correction Using Interleaved Double Spin-Echo Diffusion MRI [Internet]. Descoteaux M, Maier-Hein L, Franz A, Jannin P, Collins DL, Duchesne S, editors. MICCAI 2017. Cham: Springer International Publishing; 2017. doi:10.1007/978-3-319-66182-7

17.   Zun Z, Limperopoulos C. Placental perfusion imaging using velocity-selective arterial spin labeling. Magn Reson Med. 2018; doi:10.1002/mrm.27100

18.   Manganaro L, Fierro F, Tomei A, La Barbera L, Savelli S, Sollazzo P, et al. MRI and DWI: feasibility of DWI and ADC maps in the evaluation of placental changes

during gestation. Prenat Diagn. 2010;30: 1178–1184. Available: http://doi.wiley.com/10.1002/pd.2641

19. Bonel HM, Stolz B, Diedrichsen L, Frei K, Saar B, Tutschek B, et al. Diffusion-weighted MR Imaging of the Placenta in Fetuses with Placental Insufficiency. Radiology. Radiological Society of North America, Inc.; 2010;257: 810–819. doi:10.1148/radiol.10092283

20. Sivrioglu AK, Ozcan UA, Turk A, Ulus S, Yildiz ME, Sonmez G, et al. Evaluation of placenta with relative apparent diffusion coefficient and relative T2 signal intensity analysis. Diagnostic Interv Radiol. 2013;19: 495–500. doi:10.5152/dir.2013.13106

21. Song F, Wu W, Qian Z, Zhang G, Cheng Y. Assessment of the Placenta in Intrauterine Growth Restriction by Diffusion-Weighted Imaging and Proton Magnetic Resonance Spectroscopy. Reprod Sci. 2017;24: 575–581. doi:10.1177/1933719116667219

22. Javor D, Nasel C, Schweim T, Dekan S, Chalubinski K, Prayera D. In vivo assessment of putative functional placental tissue volume in placental intrauterine growth restriction (IUGR) in human fetuses using diffusion tensor magnetic resonance imaging. Placenta. Elsevier Ltd; 2013;34: 676–680. doi:10.1016/j.placenta.2013.04.018

23. Slator PJ, Hutter J, McCabe L, Gomes ADS, Price AN, Panagiotaki E, et al. Placenta microstructure and microcirculation imaging with diffusion MRI. Magn Reson Med. 2017; doi:10.1002/mrm.27036

24. Solomon E, Avni R, Hadas R, Raz T, Garbow JR, Bendel P, et al. Major mouse placental compartments revealed by diffusion-weighted MRI, contrast-enhanced MRI, and fluorescence imaging. Proc Natl Acad Sci. 2014;111: 10353–8. doi:10.1073/pnas.1401695111

25. Kingdom J, Huppertz B, Seaward G, Kaufmann P. Development of the placental villous tree and its consequences for fetal growth. Eur J Obstet Gynecol Reprod Biol. 2000;92: 35–43. doi:10.1016/S0301-2115(00)00423-1

26. McKenna D, Tharmaratnam S, Mahsud S, Dornan J. Ultrasonic evidence of placental calcification at 36 weeks' gestation: Maternal and fetal outcomes. Acta Obstet Gynecol Scand. Wiley/Blackwell (10.1111); 2005;84: 7–10. doi:10.1111/j.0001-6349.2005.00563.x

27. Chen KH, Chen LR, Lee YH. Exploring the relationship between preterm placental calcification and adverse maternal and fetal outcome. Ultrasound Obstet Gynecol. Wiley-Blackwell; 2011;37: 328–334. doi:10.1002/uog.7733

28. Chen KH, Chen LR, Lee YH. The Role of Preterm Placental Calcification in High-Risk Pregnancy as a Predictor of Poor Uteroplacental Blood Flow and Adverse Pregnancy Outcome. Ultrasound Med Biol. Elsevier; 2012;38: 1011–1018. doi:10.1016/j.ultrasmedbio.2012.02.004

29. Moore RJ, Issa B, Tokarczuk P, Duncan KR, Boulby P, Baker PN, et al. In vivo intravoxel incoherent motion measurements in the human placenta using echo-planar imaging at 0.5 T. Magn Reson Med. 2000;43: 295–302. doi:10.1002/(SICI)1522-2594(200002)43:2<295::AID-MRM18>3.0.CO;2-2

30. Moore RJ, Strachan BK, Tyler DJ, Duncan KR, Baker PN, Worthington BS, et al. In utero Perfusing Fraction Maps in Normal and Growth Restricted Pregnancy Measured Using IVIM Echo-Planar MRI. Placenta. 2000;21: 726–732. doi:10.1053/plac.2000.0567

31. Capuani S, Guerreri M, Antonelli A, Bernardo S, Porpora MG, Giancotti A, et al. Diffusion and perfusion quantified by Magnetic Resonance Imaging are markers of human placenta development in normal pregnancy. Placenta. Elsevier Ltd; 2017;58: 33–39. doi:10.1016/j.placenta.2017.08.003

32.   Sohlberg S, Mulic-Lutvica A, Olovsson M, Weis J, Axelsson O, Wikström J, et al. Magnetic resonance imaging-estimated placental perfusion in fetal growth assessment. Ultrasound Obstet Gynecol. John Wiley & Sons, Ltd; 2015;46: 700–705. doi:10.1002/uog.14786

33.   Sohlberg S, Mulic-Lutvica A, Lindgren P, Ortiz-Nieto F, Wikström AK, Wikström J. Placental perfusion in normal pregnancy and early and late preeclampsia: A magnetic resonance imaging study. Placenta. Elsevier Ltd; 2014;35: 202–206. doi:10.1016/j.placenta.2014.01.008

34.   Derwig I, Lythgoe DJ, Barker GJ, Poon L, Gowland P, Yeung R, et al. Association of placental perfusion, as assessed by magnetic resonance imaging and uterine artery Doppler ultrasound, and its relationship to pregnancy outcome. Placenta. Elsevier Ltd; 2013;34: 885–891. doi:10.1016/j.placenta.2013.07.006

35.   You W, Andescavage N, Zun Z, Limperopoulos C. Semi-automatic segmentation of the placenta into fetal and maternal compartments using intravoxel incoherent motion MRI. Proc SPIE 10137, Med Imaging 2017 Biomed Appl Mol Struct Funct Imaging. 2017; 1013726. doi:10.1117/12.2254610

36.   Siauve N, Hayot PH, Deloison B, Chalouhi GE, Alison M, Balvay D, et al. Assessment of human placental perfusion by intravoxel incoherent motion MR imaging. J Matern Neonatal Med. Informa UK Ltd.; 2017;0: 1–8. doi:10.1080/14767058.2017.1378334

37.   Jakab A, Tuura RL, Kottke R, Ochsenbein-Kölble N, Natalucci G, Nguyen TD, et al. Microvascular perfusion of the placenta, developing fetal liver, and lungs assessed with intravoxel incoherent motion imaging. J Magn Reson Imaging. 2017; doi:10.1002/jmri.25933

38.   Panagiotaki E, Schneider T, Siow B, Hall MG, Lythgoe MF, Alexander DC. Compartment models of the diffusion MR signal in brain white matter: A taxonomy and comparison. Neuroimage. Elsevier Inc.; 2012;59: 2241–2254. doi:10.1016/j.neuroimage.2011.09.081

39.   Slator PJ, Hutter J, Panagiotaki E, Jackson L, Santos Gomes A Dos, Ho A, et al. Optimised B-Values & Gradient Directions for Placental Diffusion MRI. ISMRM Workshop on MRI of the Placenta. 2018.

40.   Guyader JM, Bernardin L, Douglas NHM, Poot DHJ, Niessen WJ, Klein S. Influence of image registration on apparent diffusion coefficient images computed from free-breathing diffusion MR images of the abdomen. J Magn Reson Imaging. 2015;42: 315–330. doi:10.1002/jmri.24792

41.   Burton GJ, Jauniaux E. What is the placenta? Am J Obstet Gynecol. Elsevier Inc.; 2015;213: S6.e1-S6.e4. doi:10.1016/j.ajog.2015.07.050

42.   Moore RJ, Ong SS, Tyler DJ, Duckett R, Baker PN, Dunn WR, et al. Spiral artery blood volume in normal pregnancies and those compromised by pre-eclampsia. NMR Biomed. 2008;21: 376–380. doi:10.1002/nbm.1199

43.   Christen T, Lemasson B, Pannetier N, Farion R, Remy C, Zaharchuk G, et al. Is T2* Enough to Assess Oxygenation? Quantitative Blood Oxygen Level–Dependent Analysis in Brain Tumor. Radiology. 2012;262: 495–502. doi:10.1148/radiol.11110518

44.   Sinding M, Peters DA, Frøkjaer JB, Christiansen OB, Petersen A, Uldbjerg N, et al. Placental magnetic resonance imaging T2* measurements in normal pregnancies and in those complicated by fetal growth restriction. Ultrasound Obstet Gynecol. John Wiley & Sons, Ltd; 2016;47: 748–754. doi:10.1002/uog.14917

45.   Lo JO, Roberts VHJ, Schabel MC, Wang X, Morgan TK, Liu Z, et al. Novel Detection of Placental Insufficiency by Magnetic Resonance Imaging in the Nonhuman Primate. Reprod Sci. 2017; 193371911769970. doi:10.1177/1933719117699704

46.   Duncan KR, Gowland P, Francis S, Moore R, Baker PN, Johnson IR. The investigation of placental relaxation and estimation of placental perfusion using echo-planar magnetic resonance imaging. Placenta. 1998;19: 539–543. doi:10.1016/S0143-4004(98)91048-7

47.   Wright C, Morris DM, Baker PN, Crocker IP, Gowland PA, Parker GJ, et al. Magnetic resonance imaging relaxation time measurements of the placenta at 1.5 T. Placenta. Elsevier Ltd; 2011;32: 1010–1015. doi:10.1016/j.placenta.2011.07.008

48.   Derwig I, Barker GJ, Poon L, Zelaya F, Gowland P, Lythgoe DJ, et al. Association of placental T2relaxation times and uterine artery Doppler ultrasound measures of placental blood flow. Placenta. Elsevier Ltd; 2013;34: 474–479. doi:10.1016/j.placenta.2013.03.005

49.   Ingram E, Hawkins L, Morris DM, Myers J, Sibley CP, Johnstone ED, et al. R1 changes in the human placenta at 3 T in response to a maternal oxygen challenge protocol. Placenta. 2016;39: 151–153. doi:10.1016/j.placenta.2016.01.016

50.   Melbourne A, Pratt R, Owen D, Sokolska M, Bainbridge A, Atkinson D, et al. DECIDE: Diffusion-rElaxation Combined Imaging for Detailed Placental Evaluation. Proc Intl Soc Mag Reson Med 25. 2017. p. 4800.